Evaluating Trends and Seasonality in Modeled $PM_{2.5}$ Concentrations Using Empirical Mode Decomposition

Huiying Luo[1], Marina Astitha[1*], Christian Hogrefe[2], Rohit Mathur[2], S. Trivikrama Rao[1,3]

[1]University of Connecticut, Department of Civil and Environmental Engineering, Storrs-Mansfield, CT, USA
[2]U.S. Environmental Protection Agency, Research Triangle Park, NC, USA
[3]North Carolina State University, Raleigh, NC, USA

*Corresponding author: Marina Astitha, Civil and Environmental Engineering, University of Connecticut, 261 Glenbrook Road, Storrs, CT, 06269-3037, Phone: 860-486-3941, Fax: 860-486-2298, Email: marina.astitha@uconn.edu.

Abstract. Regional-scale air quality models are being used for studying the sources, composition, transport, transformation, and deposition of fine particulate matter ($PM_{2.5}$). The availability of decadal air quality simulations provides a unique opportunity to explore sophisticated model evaluation techniques rather than relying solely on traditional operational evaluations. In this study, we propose a new approach for process-based model evaluation of speciated $PM_{2.5}$ using improved Complete Ensemble Empirical Mode Decomposition with Adaptive Noise (improved CEEMDAN) to assess how well version 5.0.2 of the coupled Weather Research and Forecasting model - Community Multiscale Air Quality model (WRF-CMAQ) simulates the time-dependent long-term trend and cyclical variations in the daily average $PM_{2.5}$ and its species, including sulfate (SO_4), nitrate (NO_3), ammonium (NH_4), chloride (Cl), organic carbon (OC), and elemental carbon (EC). The utility of the proposed approach for model evaluation is demonstrated using $PM_{2.5}$ data at three monitoring locations. At these locations, the model is generally more capable of simulating the rate of change in the long-term trend component than its absolute magnitude. Amplitudes of the sub-seasonal and annual cycles of total $PM_{2.5}$, SO_4, and OC are well reproduced. However, the time-dependent phase difference in the annual cycles for total $PM_{2.5}$, OC, and EC reveal a phase shift of up to half year, indicating the need for proper temporal allocation of emissions and for updating the treatment of organic aerosols compared to the model version used for this set of simulations. Evaluation of sub-seasonal and inter-annual variations indicates that CMAQ is more capable of replicating the sub-seasonal cycles than inter-annual variations in magnitude and phase.

Keywords

Model evaluation, coupled WRF-CMAQ, improved Complete Ensemble Empirical Mode Decomposition (EMD) with Adaptive Noise, Speciated $PM_{2.5}$, Scale Separation, Seasonality, Trend

1 Introduction

It is well recognized that inhalable fine particulate matter ($PM_{2.5}$) adversely impacts human health and the environment. Regional-scale air quality models are being used in health impact studies and decision-making related to $PM_{2.5}$. Long-term model simulations of $PM_{2.5}$ concentrations using regional air quality models are essential to identify long-term trends and cyclical variations such as annual cycles in areas larger than what is covered by in-situ measurements. However, total $PM_{2.5}$ concentrations are challenging to predict because of the dependence on the contributions from individual $PM_{2.5}$ components, such as sulfates, nitrates, carbonaceous species, and crustal elements. In this context, a detailed process-based evaluation of the simulated speciated $PM_{2.5}$ must be carried out to ensure acceptable replication of observations so model users can have confidence in using regional air quality models for policy-making. Furthermore, process-based information can be useful for making improvements to the model.

Some of the trend or step change evaluations of regional air quality models in the past have focused on specific pairs of years (Kang et al., 2013; Zhou et al., 2013; Foley et al., 2015). These studies do not properly account for the sub-seasonal and inter-annual variations between those specific periods. Trend evaluation is commonly done by linear regression of indexes such as the annual mean or specific percentiles, assuming linearity and stationarity of time series (Civerolo et al., 2010; Hogrefe et al., 2011; Banzhaf et al., 2015; Astitha et al., 2017). The problem with the linear trend evaluation is that there is no guarantee the trend is actually linear during the period of the study because the underlying processes are in fact nonlinear and nonstationary (Wu et al., 2007).

Seasonal variations are usually studied and evaluated by investigating the monthly or seasonal means of total and/or speciated $PM_{2.5}$ (Civerolo et al., 2010; Banzhaf et al., 2015; Yahya et al., 2016; Henneman et al., 2017). Evaluation of ten-year averaged monthly mean (i.e., ten-year averaged mean in Jan., …, Dec.) of $PM_{2.5}$ simulated with WRF/Chem against the Interagency Monitoring of Protected Visual Environments (IMPROVE) by Yahya et al. (2016) shows that the model captures the observed features of summer peaks in $PM_{2.5}$ with a phase shift of few months. However, according to the analysis (Fig. 10) in Henneman et al. (2017), the seasonality shown in monthly-averaged $PM_{2.5}$ time series is much less distinguishable compared with that of ozone and CMAQ (version 5.0.2) does not replicate the monthly $PM_{2.5}$ quite well with large underestimation in the summer months. In these studies, the seasonality might not be well represented by the preselected averaging window size of one or three months. In addition, averaging of those monthly or seasonal means across multiple years may conceal the long-term trends or interannual variations driven by climate change, emission control policies or other slow varying processes.

To address the above-mentioned problems, we propose a new method for conducting air quality model evaluation for $PM_{2.5}$ using improved CEEMDAN. Improved CEEMDAN is an Empirical Mode Decomposition (EMD)-based, data-driven intrinsic mode decomposition technique that can adaptively and recursively decompose a nonlinear and nonstationary signal into multiple modes called intrinsic mode functions (IMFs) and a residual (trend component) (Huang et al., 1998; Wu and Huang, 2009; Yeh et al., 2010; Torres et al., 2011; Colominas et al., 2014). It does not require any preselection of the temporal scales or assumptions of linearity and stationarity for the data, thereby providing some insights into time series of $PM_{2.5}$ concentrations and its components. Decomposed $PM_{2.5}$ long-term trend components and annual cycles from observed and simulated $PM_{2.5}$ serve as the intuitive carrier of the trend and

seasonality evaluation. In the meantime, several other IMFs with characteristic time scales ranging from multiple days to years are also decomposed, enabling model evaluation of the less studied sub-seasonal and inter-annual variations.

2 Coupled WRF-CMAQ $PM_{2.5}$ Simulations and Observations

The two-way coupled WRF-CMAQ (version 5.0.2) is configured with a 36 km horizontal grid spacing over the contiguous United States (CONUS) with 35 vertical layers of varying thickness extending from the surface to 50 mb (Wong et al., 2012; Gan et al., 2015). Time-varying chemical lateral boundary conditions were derived from the 108 km resolution hemispheric WRF-CMAQ (Mathur et al., 2017) simulation for the 1990-2010 period (Xing et al., 2015). The simulations are driven by a comprehensive emission dataset which includes aerosol precursors and primary particulate matter (Xing et al., 2013, 2015). Annual emissions for the CMAQ simulations were estimated using the methodology described in Xing et al. (2013). Briefly, the National Emissions Inventory (NEI) for 1990, 1995, 1996, 1999, 2001, 2002, and 2005 and a number of sector-specific long-term databases containing information about trends in activity data and emission controls were used to create county-level annual emissions for a total of 49 emission sectors. Prior to being used as input to the CMAQ simulations, these annual emissions were then temporally and spatially allocated to provide hourly emissions based on monthly, weekly, and diurnal temporal cross-reference and profile data from the 2005 NEI modeling platform. These profile data vary by emission sources and sometimes by state and county and are generally based on surveys and extrapolation of activity data which can be subject to uncertainty. Exceptions to the use of 2005 NEI platform temporal profile data for temporal allocation were emissions from electric generating units (EGU) which directly used measured hourly emissions after 1995 and wildfire emissions that used climatological monthly, weekly, and diurnal profiles for temporal allocation. Readers can refer to Gan et al. (2015) for additional model information and the trend evaluation against seven pairs of sites from the CASTNET (Clean Air Status and Trend Network) and IMPROVE networks for 1995-2010. We obtained the 2002-2010 daily average $PM_{2.5}$ and its speciated time series from the set of simulations with direct aerosol feedback. The earlier years of 1990-2001 are not included in this evaluation because of the limited availability of speciated $PM_{2.5}$ observations.

To avoid misinterpretation of data due to the presence of missing values, only sites with continuous complete long-term record for total $PM_{2.5}$ and its speciation including SO_4, NO_3, NH_4, OC, EC, and Cl are studied (Fig. 1). All of the selected sites have data coverage above 90% each year for at least six consecutive years between 2002 and 2010 (equivalent to 30% for 1-in-3 days sampling sites). This strict data selection led to the sparsity of this type of observations for the study period. QURE, a rural site carrying out 1-in-3 days sampling of total and speciated $PM_{2.5}$ of SO_4, NO_3, OC, EC, and Cl, is located in Quabbin Summit, MA. It is one of the three sites from the IMPROVE network that has at least six continuous years of speciated observations and was selected here to demonstrate the application of the proposed method in rural areas. It should be noted that the majority of the observed Cl in 2002 and 2003 is negative due to a filter issue which was not addressed until 2004 (White, 2008). Thus, simulations of Cl are only evaluated during 2004-2007 at this site. Station RENO, located in urban Reno, NV, is also a 1-in-3 days sampling site of total and speciated $PM_{2.5}$ of SO_4, NO_3, NH_4, OC, and EC, and it is the only Chemical Speciation Network (CSN) site that fulfills this data coverage requirement. The third site ATL in the Southeastern Aerosol Research and Characterization Study (SEARCH) network is located 4.2 km northwest of downtown Atlanta, GA. It is the only long-

term site available with daily sampling (Hansen et al., 2003; Edgerton et al., 2005) that meets the data coverage requirement. The best-estimate (BE), a calculated concentration intended to represent what is actually in the atmosphere (Edgerton et al., 2005), of the total $PM_{2.5}$ and SO_4, NO_3, NH_4, and EC components are retrieved for the evaluation. OC component is a direct measurement. These three sites have a continuous record covering at least 6 years (2002 – 2007 for QURE and ATL, 2002 – 2010 for RENO) that allows an evaluation of long-term trends.

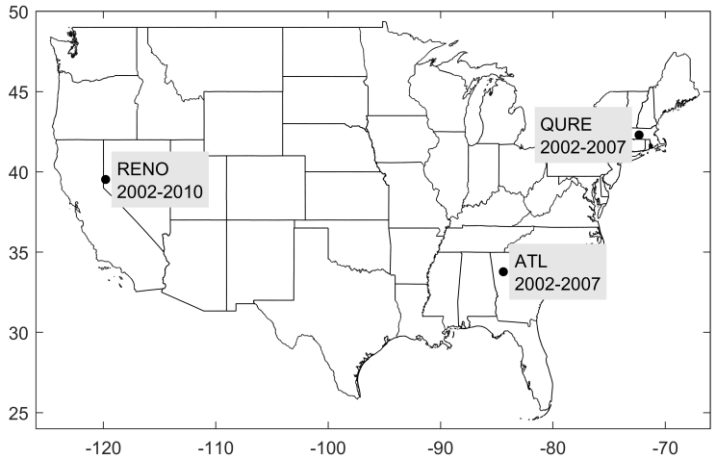

Fig. 1. Location and data coverage of the $PM_{2.5}$ monitoring sites QURE, RENO, and ATL.

3 Methodology

3.1 Empirical Mode Decomposition

The Empirical Mode Decomposition (EMD) technique, proposed in the late 1990s, is capable of adaptively and recursively decomposing a signal into multiple modes called intrinsic mode functions (IMFs), where each mode has a characteristic frequency, and a residual with one extremum at most (Huang et al., 1998). EMD decomposes the original signal into several IMFs and a residual through a repeated process called "sifting": first, local maxima and minima are identified and interpolated separately with a cubic spline as the upper and lower envelop; then an IMF candidate is derived by subtracting the mean of the envelops from the original signal. If the candidate satisfies the following criteria (Huang et al., 1998), it is saved as the first IMF (IMF1), and the remaining portion (original signal – IMF1) is treated as a new input signal for the decomposition of the remaining IMFs; otherwise, more sifting processes should be carried out until the candidate becomes an IMF.

1) The number of extrema (maxima and minima) and the number of zero-crossings must be equal or differ at most by one; 2) The local mean at any point, the mean of the envelope defined by local maxima and the envelope defined by local minima, must be zero.

In this way, IMF1, IMF2, … are decomposed recursively with decreasing characteristic frequency. The final remaining residual (trend) could be a monotonic function of time or a long-term component with one extremum at most. The decomposed signal then is expressed as the summation of all IMFs and the final residual:

$$x = \sum_{i=1}^{k} d_i + r \quad (1)$$

where x is the original signal, d_i is the i^{th} IMF, k is the total number of IMFs and r is the final residual.

Nevertheless, "mode mixing", where oscillations with very disparate scales can be present in one mode or vice versa, is commonly reported. To cope with this issue, multiple noise assisted EMD have been developed successively (Wu and Huang, 2009; Yeh et al., 2010; Torres et al., 2011; Colominas et al., 2014). It is evident that the latest improved Complete Ensemble EMD with Adaptive Noise (improved CEEMDAN) manages to alleviate the problem of mode mixing with the benefit of reducing the amount of noise presented and avoiding spurious modes (Colominas et al., 2014). Moreover, the end effects or boundary effects have been addressed by its predecessor EEMD (Ensemble Empirical Mode Decomposition) by extrapolating the maxima and minima, and behaved well in numerous time series with dramatically variant characteristics (Wu and Huang, 2009). The extrapolation of maxima and minima is proven to be more effective compared with the extrapolation of the signal itself such as repetition or reflection (Rato et al., 2008).

Given the EMD's ability to deal with real-world nonstationary and nonlinear time series, it is widely used in engineering, economics, earth, and environmental sciences (e.g., Huang et al., 1998; Chang et al., 2003; Yu et al., 2008; Colominas et al., 2014; Derot et al., 2016). We use the most up-to-date noise-assisted improved CEEMDAN technique with at least hundreds of noise realizations to decompose observed and simulated $PM_{2.5}$ time series. Readers can refer to Colominas et al. (2014) for a detailed description of the technique and access to the corresponding MATLAB code. Trial and error attempts are made in setting the inputs (standard deviation of the added noise and the limit of maximum number of sifting allowed) of the improved CEEMDAN function to achieve best mode separation. In a desired best mode separation, neighboring IMFs should have very limited levels of mode mixing, which can be fast screened based on the time series of the decomposed IMFs and their power spectrum.

The impact of boundaries on the decomposed annual cycles and the residual is assessed by the variations (standard deviation) of hypothetical decomposed boundaries by cutting a continuous eighteen-year total $PM_{2.5}$ observation (North Little Rock, AR) 48 times at different years and times of the year (Fig. S1). The standard deviation of the annual cycles is found to largely diminish within half the annual cycles and could be negligible within one year. This could very possibly expand to IMFs with other characteristic scales. Yet, trend components (residuals) show variability depending on the available time period after cutting. Most of the time, they follow the reference long-term trend reflected either by the residual or the summation of the residual and the IMF with the longest temporal scale decomposed from the eighteen-year $PM_{2.5}$ (Fig. S1c). This is in line with our expectations as a trend should exist within a given time span, following the definition in Wu et al. (2007): "The trend is an intrinsically fitted monotonic function or a function in which there can be at most one extremum within a given data span".

Although very strict data completeness requirement is employed for this study, it should not be conceived as a limitation of the method itself. A sensitivity test based on a period of nine years of total $PM_{2.5}$ observations at the same site with 99% data coverage shows that even though variability of annual cycles and long-term trends increases with decreased data availability (100%, 90%..., 10%), the structure of those components is consistent. The average of 40 realizations of annual cycles and long-term trend components in each data-completeness scenario is in perfect

alignment with that of 100% data completeness (Fig. S2 and S3). Given the fact that those 40 realizations in each scenario are based on independent random samplings of the original observations, the increased variability could very possibly result from the difference in the sampled data itself rather than the method. Thus, the robustness of improved CEEMDAN decomposed annual cycles and long-term trend is justified. In fact, EMD has been proven to be an effective tool for data gap-filling (Moghtaderi et al., 2012).

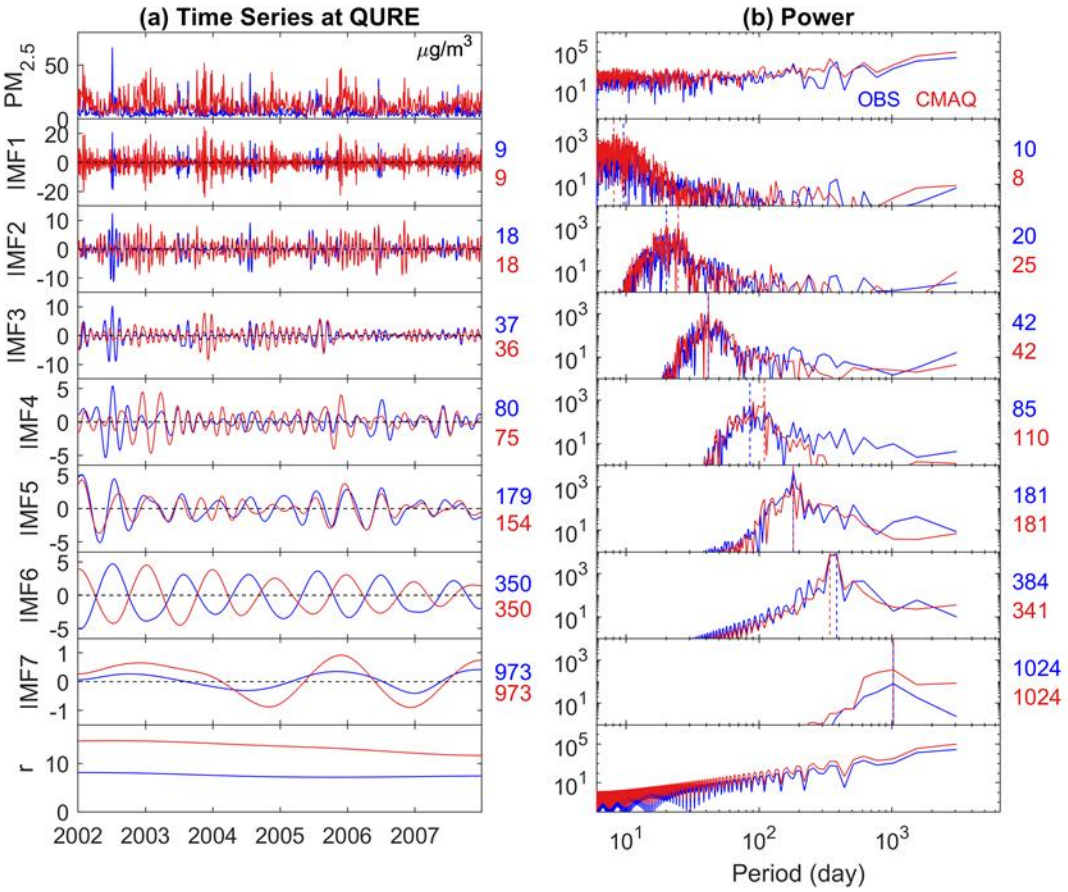

Fig. 2. Decomposition of observed (blue) and simulated (red) 24-hour average total $PM_{2.5}$ into 7 IMFs and a residual component (trend) at Quabbin Summit, MA using the improved CEEMDAN: (a) Time series of total $PM_{2.5}$, IMFs, and the residual component (all with the unit of μg/m^3); (b) Power spectrum of the corresponding time series. The colored numbers on the right side of time series are the mean period t_m in days, while the ones on the right side of the power spectrum are the peak period t_p in days, which are also indicated by the dashed vertical lines on the power spectrum. Note that the scales for the time series are not all the same. Also, all power spectra are in the log scale, and those of the IMFs are zoomed in with a range of 10^0 to 10^4 on the y-scale for better visual clarity (compared with 10^{-2} to 10^7 for total $PM_{2.5}$ and the residual component).

The characteristic period of each IMF can be estimated by the peak period t_p (days) where the power spectrum of the IMF peaks:

$$t_p = \frac{1}{f_p} \qquad (2)$$

in which f_p is the frequency that the power spectrum peaks in the unit of number of cycles per day. The peak estimates can be biased if more than one high-power frequency is located closely within one IMF. Thus, the power spectrum and t_p is only used as a fast screening tool to determine if a desired decomposition is accomplished. As an alternative approach, the mean period t_m can be estimated by:

$$t_m = \frac{Time\ span}{(n_{max}+n_{min}+n_{zero})/4} \qquad (3)$$

where n_{max} , n_{min}, and n_{zero} are the number of maxima, minima, and zero-crossings, respectively, during the $Time\ span$ (days). As the frequency decreases, the mean period estimates become less accurate because of the limited time span compared with the length of the cycle and should be carefully interpreted.

An example of the total $PM_{2.5}$ decomposition with improved CEEMDAN at the QURE site shows modes ranging from very high frequency to very low frequency (IMF1 to IMF7) and a residual (Fig. 2). No visible mode mixing can be detected in both the time series (Fig. 2a) and the power spectrum (Fig. 2b) of all IMFs. Mean (t_m) and peak (t_p) estimations of the characteristic periods of each IMF are presented on the right side of each mode. Annual cycles and long-term trend components are well represented by IMF6 and the residual, with the remaining IMFs carrying weekly, sub-seasonal, seasonal, and inter-annual variations, respectively, for both observed and simulated $PM_{2.5}$ (Fig. 2). We have noticed that in some rare cases, a spurious mode in the last IMF with synchronous signal and very close scales to its previous IMF exists. This is possibly due to the fact that the characteristic periods of those IMFs are in proximity to the span of the studied time span. In these cases, the last two modes are merged by adding them together to conduct a detailed evaluation as discussed in Section 4.1.

3.2 Statistical metrics

EMD-decomposed IMFs and trend components allow for a detailed time-dependent evaluation of $PM_{2.5}$ and provide a novel opportunity to trace the performances of specific scales back to the corresponding speciated components. Note that the trend component is the decomposed residual component from the $PM_{2.5}$ in the unit of $\mu g/m^3$, and it is not the traditional concept of trend in concentration per time. In addition to a direct evaluation of its magnitude, we also calculated its derivative to identify the periods with higher or lower rate of change (concentration per time). Time-dependent intrinsic correlation (TDIC) is utilized to study the evolvement of the model performance for cyclic variations throughout time (Chen et al., 2010; Huang and Schmitt, 2014; Derot et al., 2016). It is a set of correlations calculated for IMFs over a local period of time I centered around time t:

$$I(t) = [t - \frac{t_w}{2}, t + \frac{t_w}{2}] \qquad (4)$$

in which t is the center time for the calculation of the correlation and t_w is the moving window length. The minimum of t_w is set to be the local instantaneous period of the IMF (larger of that in observation or simulation) using the general zero-crossing method to ensure that at least one instantaneous period is included in calculating the local

correlation coefficient (Chen et al., 2010). The maximum of t_w is the entire data period with a traditional overall correlation being calculated. The empty spaces in the pyramids used to depict the TDIC are an indication that the correlation is not statistically significantly different from zero. With both decomposed observed and modeled concentrations in a narrow scale range, the correlation would no longer be contaminated by coexisting signals of different scales (Chen et al., 2010).

In order to summarize the performance of the decomposed trend components and IMFs, the ratio of the mean magnitudes of the trend components is defined as:

$$r_{trend} = \frac{Mean_{CMAQ}}{Mean_{observation}} \qquad (5)$$

where $Mean_{CMAQ}$ and $Mean_{observation}$ represent the mean of simulated and observed residual components respectively. The ratio of the mean amplitude of each IMF is defined by Equation 6, where an example for the annual cycles is provided:

$$r_{annual} = \frac{RMS_{CMAQ,annual}}{RMS_{observation,annual}} \qquad (6)$$

where $RMS_{observation,annual}$ and $RMS_{CMAQ,annual}$ represent the root mean square of observed and simulated annual cycles respectively. Finally, the phase shift of an IMF n is defined as the days an IMF decomposed from modeled time series has to be shifted to maximize the correlation (R_{max}) with the corresponding IMF from observed $PM_{2.5}$ time series. In practice, n could be as much as a few cycles of the mean period, t_m. Here, we limit the absolute number of shift days to not exceed a half cycle as a reference for the phase shift of an IMF. Thus, n satisfies $-\left({}^{t_m}/_{2}\right) \le n \le \left({}^{t_m}/_{2}\right)$ with t_m being the larger mean period in observation or simulation. It becomes $-0.5 \le {}^{n}/_{t_m} \le 0.5$ in terms of number of cycles.

4 Results and Discussion

4.1 Temporal scales

Temporal scales in $PM_{2.5}$ resolved by EMD depend solely on the intrinsic properties of the data itself. These properties include underlying characteristics of specific $PM_{2.5}$ concentrations, the data sampling frequency, which determines the scales that can be resolved in the high frequency IMFs, and the time span for the data coverage, which could possibly play an important role in differentiating the low frequency IMFs from the trend component. Here, we first evaluate the scales represented by the mean period in the speciated and total $PM_{2.5}$ time series. Since each IMF represents a nonstationary process, the mean period t_m is only an estimate of its characteristic scale. Evaluation of t_m might not necessarily be able to identify issues with corresponding model simulations, and it does not indicate any information on the magnitude or the phase of the time series, which is more important and will be further discussed in Sections 4.3 to 4.4.

Fig. 3a presents the characteristic scales (t_m) of IMFs in observed and simulated total and speciated $PM_{2.5}$ of QURE. The CMAQ model compares well with the observations for IMFs 1 through 6 with cycles of 9, 19, 37, 78, 158 and

347 days (average of all observed and simulated total and speciated $PM_{2.5}$). Among all these IMFs, IMF6, which represents the annual cycles, shows the least variations in the characteristic scale (Fig. 3a) and highest peak energy from the power spectrum such as Fig. 2b for total $PM_{2.5}$, except for observed EC and OC where the power of half-year cycles is more dominant (Fig. S4). These two features demonstrate a clear seasonality in both observed and simulated total and speciated $PM_{2.5}$, which would otherwise be concealed by practices such as monthly averaging. This can be further confirmed by the statistical significance of the annual cycles (except for observed EC and OC) (Fig. S5) based on a Monte Carlo verified relationship between the energy density and mean period of IMFs (Wu and Huang, 2004; Wu et al., 2007). To explore the inter-annual cycles in more detail, mean periods of IMFs with scales longer than a year are being displayed in the top left panel of Fig. 3a. Some variability exists between the observation and model simulation to the extent that not all IMFs from observation are being simulated and vice versa for the inter-annual cycles. The characteristic scales of all decomposed IMFs with scales longer than a year are shown in Fig. 3d. The estimated mean periods of the inter-annual cycles and the differences in the presence of slow varying cycles with the long characteristic scales are likely to be influenced by their proximity to the data time span of 6 years (4 years for Cl). This implies that the model evaluation shouldn't go beyond 3 years (2 years for Cl) given the current data coverage. CMAQ captured the 3-year cycles in EC and total $PM_{2.5}$ and 2-year cycles in OC and Cl, despite an overestimation in the scales of 2-year cycles in observed SO_4 and NO_3.

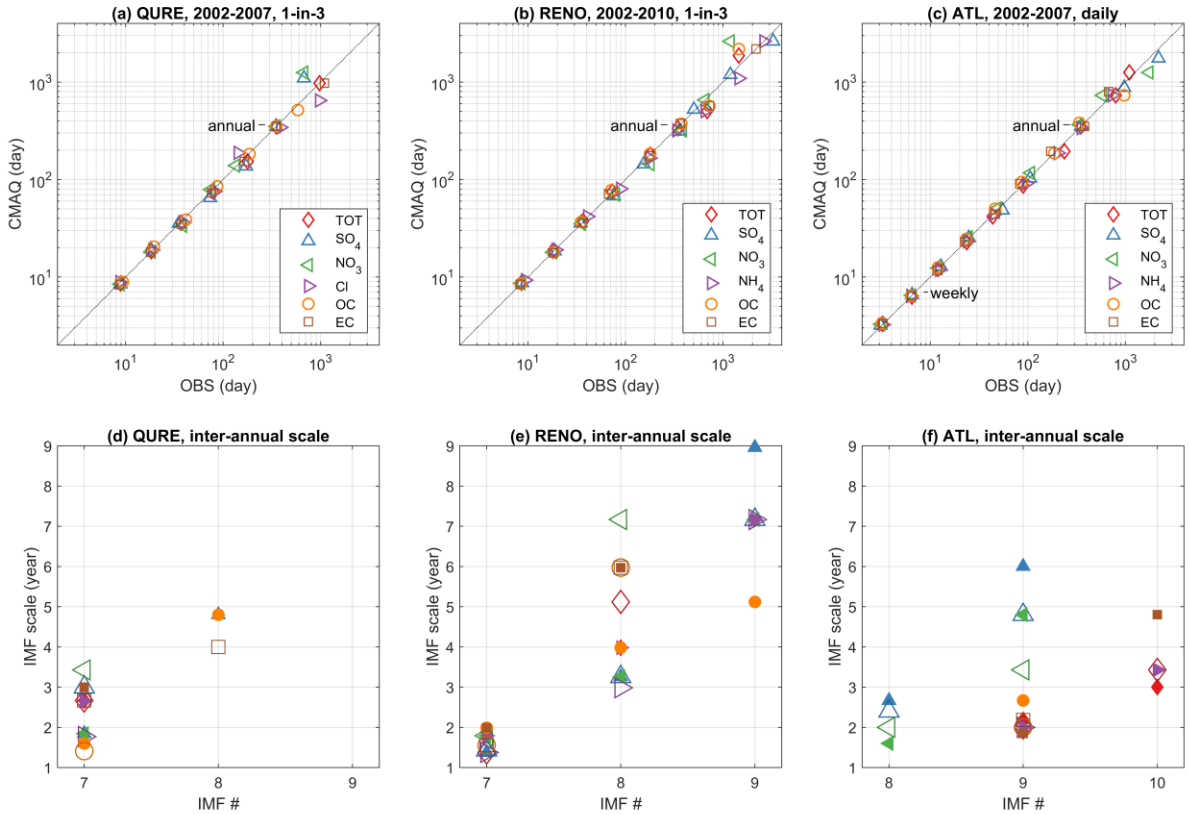

Fig. 3. The characteristic scales (t_m) resolved in the IMFs of observed and simulated total and speciated $PM_{2.5}$ for (a, d) QURE, (b, e) RENO, and (c, f) ATL. In (a-c), IMF1 to the last pair of IMFs with increasing characteristic periods are shown from bottom left to top right. Mean periods of IMFs with scales longer than a year are being displayed in (d-f) with the same shapes as in the legend above to show the characteristic scales of all decomposed IMFs given that not all IMFs from observation are being simulated and vice versa. In the (d-f), species decomposed from observations are shown with smaller filled shapes, while species decomposed from simulations are represented by larger open shapes in slightly darker shades.

Similar features in observed and simulated total and speciated $PM_{2.5}$ concentrations at RENO are presented in Fig. 3b. Likewise, the highest peaks in the power spectrum also sit in the annual cycles of IMF6 except for the observed OC and total $PM_{2.5}$ which have higher peak power at half-year cycles. All annual IMFs are statistically significant except for simulated NH_4 (Fig. S5). The small variation in the estimated characteristic period of IMF6 is because this monitoring site is located in a wildfire prone region on the border of Nevada and California. Clear evidence can be seen from Fig. 4a that an extra annual cycle in the IMF6 of observations in the summer of 2008 is depicted, which is very possibly driven by the 2008 California Wildfires spanning from May until November. Satellite image of the wildfire smoke on July 10, 2008 can be found in Figure 1 from Gyawali et al. (2009). Unlike the diversified scales in IMF7 at QURE, IMF7 at RENO features universal 2-year cycles of all species as well as total $PM_{2.5}$ and all of them are well replicated by the model. However, variations in time scales are present in IMF8 possibly because of the limited data coverage. Thus, only species with time scales less than 4 years in both observations and model simulations are evaluated. It is evident that CMAQ has reproduced the 3-year cycles in SO_4 and NH_4.

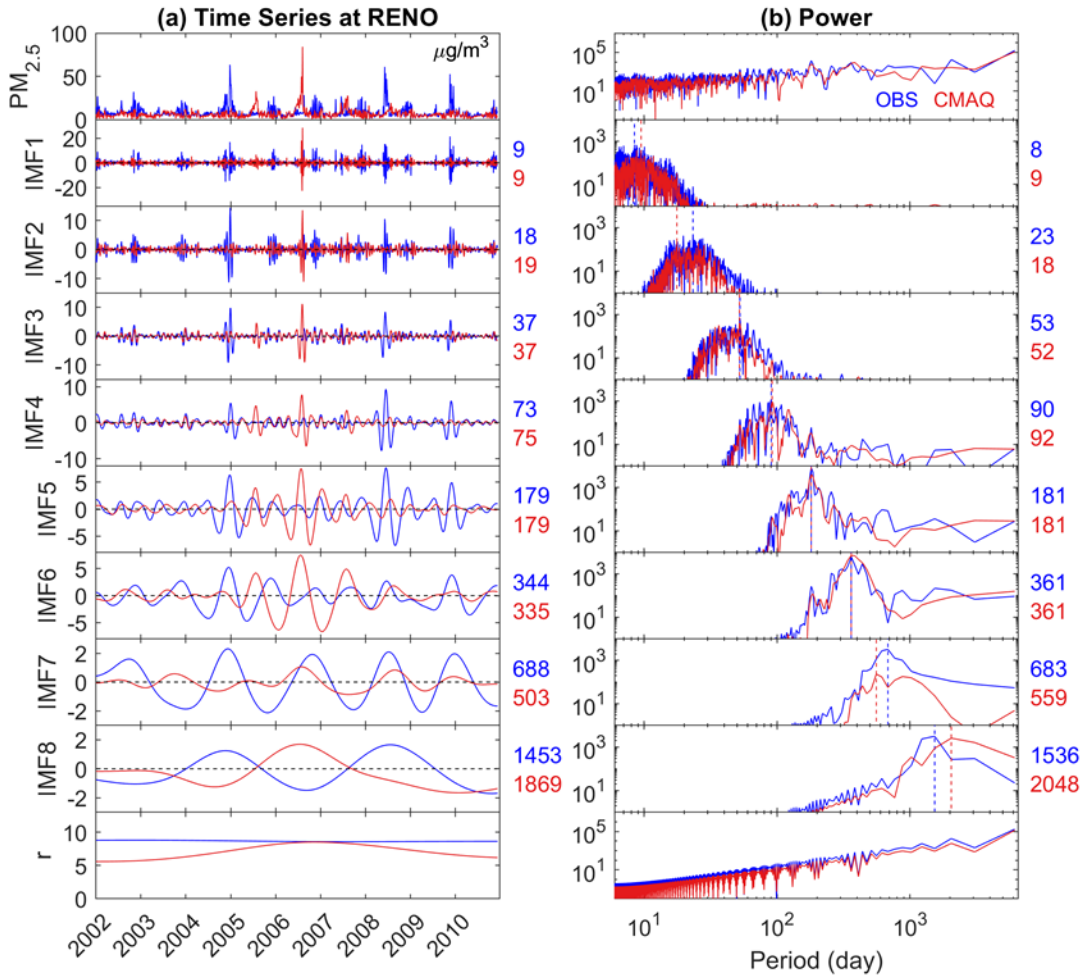

Fig. 4. Same as Fig. 2 but for the RENO site with 8 IMFs.

ATL is the only speciated site with daily data coverage. Observed and simulated total and speciated $PM_{2.5}$ concentrations at the ATL site are decomposed into 9 or 10 IMFs (Fig. 3c). Because of the change in data frequency, high frequency scales such as weekly cycles can be evaluated and the significance tested (Fig. S5) annual cycles with the highest peak power is represented by IMF8 (IMF7 for SO_4 and NO_3). Annual cycles of SO_4 and NO_3 appeared in the earlier stage of decomposition in IMF7 because of their relatively weak half-year cycles, which largely led to the mixed signal of half-year and annual cycles in IMF7 in total $PM_{2.5}$ as in Fig. 5b. This is more visible in the observed IMF7 where the energy of the one-year period surpasses that of the half-year. Yet, clues can be seen from Fig. 5 that the amplitude and the energy of annual cycles leaked into IMF7 is very limited compared to that remaining in IMF8, indicating that it is still safe to conduct model evaluation on the seasonality using IMF8 with an underestimation in the amplitude of observation. On the other hand, inferences should be made with caution for IMF7 because of the mixed modes. Scales up to 3 years are relatively well reproduced by the model.

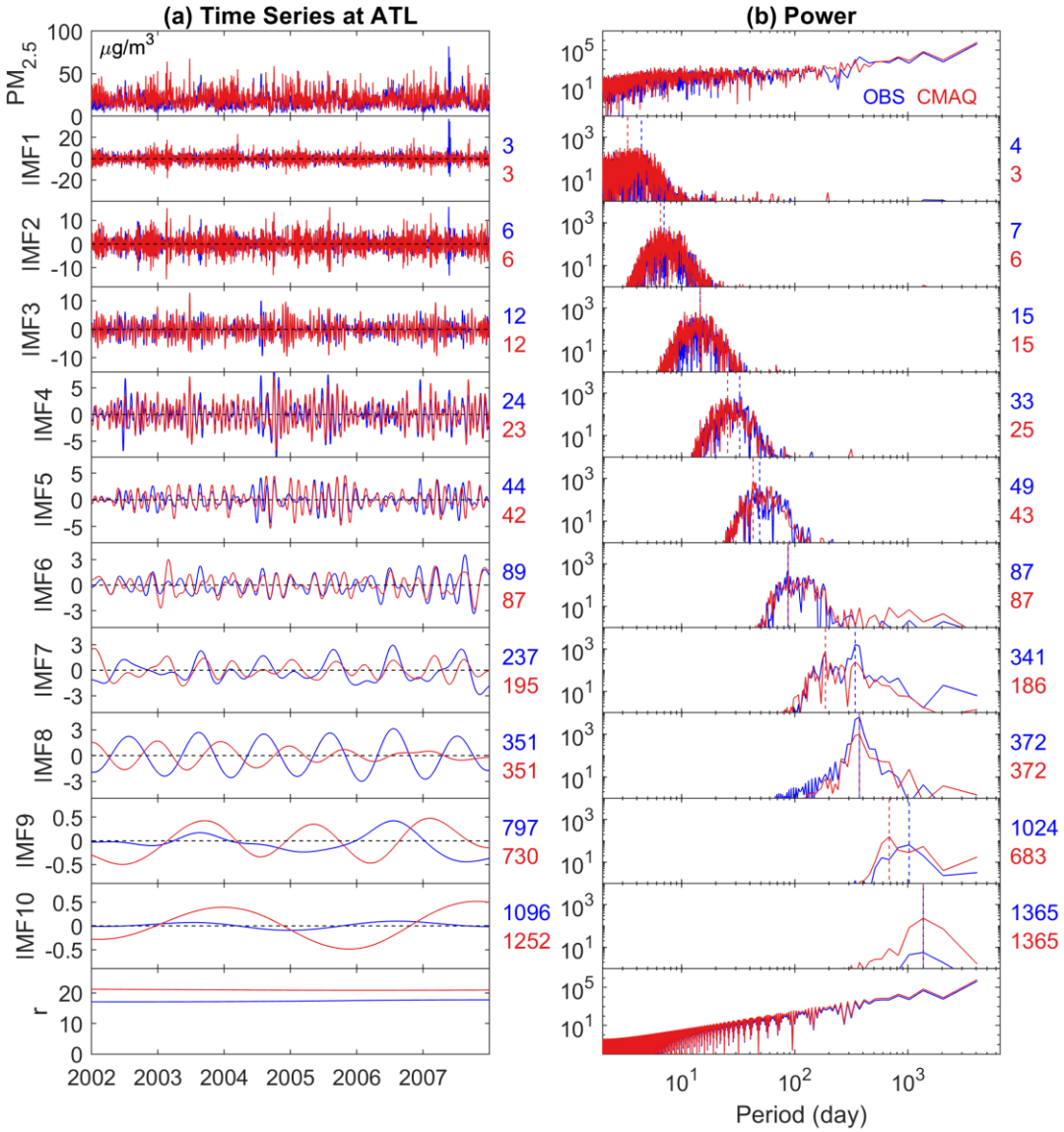

Fig. 5. Same as Fig. 2 but for the ATL site with 10 IMFs.

4.2 Long-term trend

The EMD-decomposed long-term trend components for the observed and simulated total and speciated $PM_{2.5}$ concentrations are presented in Fig. 6. To better visualize the non-linearity of the trend component, the rates of change (temporal derivative of a trend component, which is the change in the consecutive concentration divided by the sampling rate of 1 or 3 days and converted to the unit of μg/m^3/year by multiplying 365 day/year) are added with a separate y-axis on the right side in each panel (gray colored scale). It is evident that $PM_{2.5}$ is changing at a varying rate, forming either a monotonic trend component or a trend component with one extremum, which cannot be fully represented by a single constant number using a traditional linear regression approach. Given that there are chemical

species (the remaining component, *Rem*) other than the ones studied in the total $PM_{2.5}$, not all performance issues can be fully explained by the five available species.

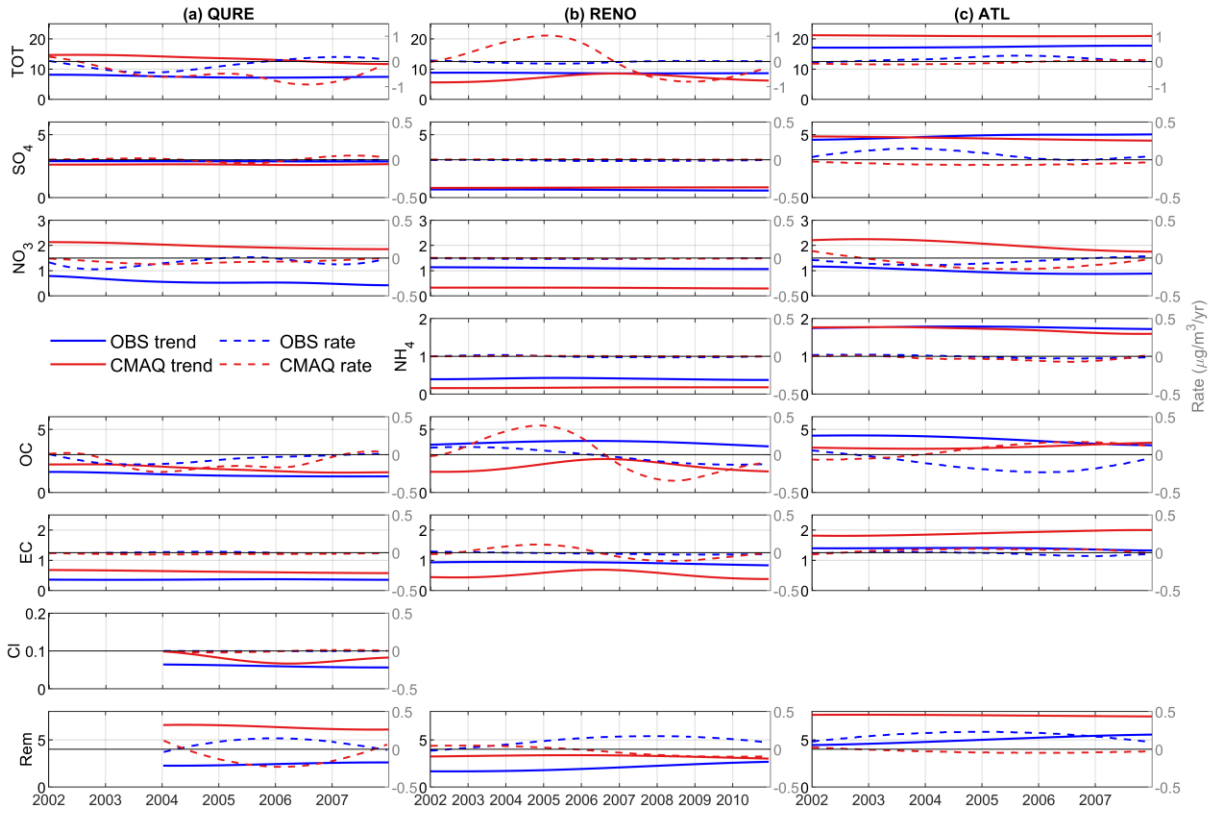

Fig. 6. Trend components of observed and simulated total and speciated $PM_{2.5}$ for (a) QURE, (b) RENO and (c) ATL in μg/m^3. Dashed lines representing the rate of the change (temporal derivative of the trend component converted to μg/m^3/year) are plotted against the right-side y axis, with a reference line of no change in black in the center. Note that the scales are not all the same.

At the QURE site, CMAQ captures the general decreasing trend in observed total $PM_{2.5}$ which can mainly be traced back to NO_3, OC, and the remaining components, while both observed and simulated trend components of SO_4 and EC are relatively constant (Fig. 6a). The relative importance of each component in driving the trend of observed and simulated total $PM_{2.5}$ reflected by its mean concentration share is summarized in Table 1 (time-dependent variations of the concentration share is attached in Fig. S6 for reference). Moreover, the periods with highest decreasing rate in observed total $PM_{2.5}$ during 2003-2004 with a decreasing rate of -0.44 μg/m^3/year is also well replicated by the model. Nevertheless, the slightly increasing $PM_{2.5}$ level in the later years is simulated to be decreasing at a much higher rate, which is partly due to the overestimated decreasing rate in OC and species other than the five studied ones. The trend component of simulated Cl shows a cyclic-like feature because of proximity between the existence of a cycle of 4-5

years (by decomposing the simulation during the 6-year study period) and 4-year period limited by the available quality assured observations. The rate of change in the simulated trend component by decomposing the simulation during the 6-year study period would mimic that from the 4-year observation, both with a negligible negative value throughout 2004-2007. However, the mean magnitude of the trend component is almost twice as high (1.8 times compared with observation) in the model with contribution from all species except for SO_4. A quantitative summary of the comparison between the mean magnitudes of the observed and model trend components can be found in Table 2.

Table 1. Concentration share (%) of different components in total $PM_{2.5}$. It is estimated by dividing the mean trend components of each species by that of total $PM_{2.5}$ for both OBS and CMAQ, multiplied by 100. The concentration share of the remainder species *Rem* is estimated by subtracting all the available species share from 100 to compensate for the small discrepancies caused by the rounding up process and uncertainty in the mode decomposition. "-" indicates the data is not available (same applies for all other tables).

		SO_4	**NO_3**	**NH_4**	**OC**	**EC**	**Cl**	**Rem**
QURE	OBS	38	7	−	19	5	1	30
	CMAQ	19	15	−	14	5	1	47
RENO	OBS	7	13	5	46	11	−	20
	CMAQ	11	4	2	30	7	−	45
ATL	OBS	28	6	10	24	8	−	24
	CMAQ	22	10	8	17	9	−	33

Table 2. The ratio of mean magnitude of the trend component r_{trend} (CMAQ/observation). Boldface values indicate a relatively good estimate of the magnitude (0.7 - 1.3).

	TOT	SO_4	NO_3	NH_4	OC	EC	Cl
QURE	1.8	**0.9**	3.5	-	1.4	1.7	**1.3**
RENO	**0.8**	**1.3**	0.3	0.4	0.5	0.6	-
ATL	**1.2**	**1.0**	2.1	**1.0**	**0.9**	1.4	-

RENO is located close to the border with California and is affected by large wildfire breakouts in the western U.S. (Gyawali et al., 2009) as can be seen in the spikes of the observed total $PM_{2.5}$ (Fig. 4a). Thus, OC makes up a much larger portion of total $PM_{2.5}$ compared to other locations (Table 1). The model simulates large increasing rate up to 1.03 μg/m^3/year and decreasing rate up to -0.80 μg/m^3/year before and after the 2006-2007 winter season and fails to reproduce the relatively stable condition seen in the observations with only -0.09 μg/m^3/year decreasing in 2004-2005 and 0.04 μg/m^3/year increasing in 2008-2009 (Fig. 6b). Similar feature is found for combustion-related OC and EC species. The observed slightly decreasing trends in SO_4 and NH_4 during 2005-2009 are not being captured in the model simulations. The magnitude of the trend component is slightly underestimated with r_{trend} of 0.8 with contribution from all species except for SO_4 as well (Table 2).

During the period of 2002-2007, observations at ATL reveal a slightly increasing $PM_{2.5}$ trend that cannot be explained by the five available $PM_{2.5}$ components trend (Fig. 6c), indicating a contribution of the remaining species such as the non-carbonaceous portion of organic matter. Non-carbonaceous organic matter can account for more than half of total organic matter, which, in turn, can account for a large portion of the total $PM_{2.5}$ mass (Edgerton et al., 2005). In contrast, the model shows a slight decreasing trend with a peak decreasing rate in 2003 and misses the peak increasing rate of 0.23 $\mu g/m^3$/year in the winter season of 2005. Similarly, reversed trends are also simulated for SO_4, OC, and EC, while the change rate in NO_3 is well captured. Unlike the previous sites, magnitude of trend components in total and speciated $PM_{2.5}$ are well simulated except for EC (1.4 times the observation) and NO_3 (2.1 times).

To sum up, the decreasing long-term trend at QURE is well simulated by the model. The occurrence of large wildfires lasting for several months has significantly impacted the long-term trend component at RENO and the model failed to capture those combustion-related species and total $PM_{2.5}$ primarily due to limitations in the historical data used to specify day-specific wildfire emissions (Xing et al., 2013). Slightly increasing levels of $PM_{2.5}$ and its species observed at ATL are simulated to be slightly decreasing, except for NO_3 which is well simulated. The magnitude of the long-term trend components of total $PM_{2.5}$ and SO_4 are well represented by CMAQ (Table 2). The model performs differently across the sites in terms of the magnitudes of the trend component in NO_3, NH_4, Cl, OC, and EC. The large discrepancy in the magnitude of some long-term trend components is likely pointing to the systematic bias in the annual emission estimations as discussed in Xing et al., (2013), which mainly focused on long-term trend rather than the absolute level of the emissions. Species other than those in the available dataset also play a considerable role in driving the agreements or disagreements between model simulations and observations of total $PM_{2.5}$.

4.3 Seasonality

The EMD-assisted seasonality evaluations utilize the decomposed IMFs with characteristic period of one year to evaluate the amplitude and phase of the model simulation, both of which are time-dependent. As mentioned in Section 4.1, these IMFs are statistically significant from white noise with few exceptions (Fig. S5). We first demonstrate the evaluation for total $PM_{2.5}$ at QURE (Fig. 7a). The top panel shows the annual cycle components and the bottom panel shows its TDIC pyramid. The decreasing amplitude of the annual cycles throughout 2002-2007 is almost perfectly represented with an overall ratio r_{annual} being 1.0 (Table 3). Each pixel in the TDIC pyramid is the correlation (color-coded) calculated during a period of time $I(t)$ with width of t_w days (y-axis) centered at a specific day (x-axis) as introduced in Section 3.2. The annual cycle mean periods are identical between CMAQ and observations (350 days, Fig. 2a IMF6), but there is a phase shift for all years with the entire TDIC pyramid being close to -1. By shifting the CMAQ annual cycles backward 159 days (almost half year), the overall correlation of the annual component can reach up to a peak of 0.9 (Table 4).

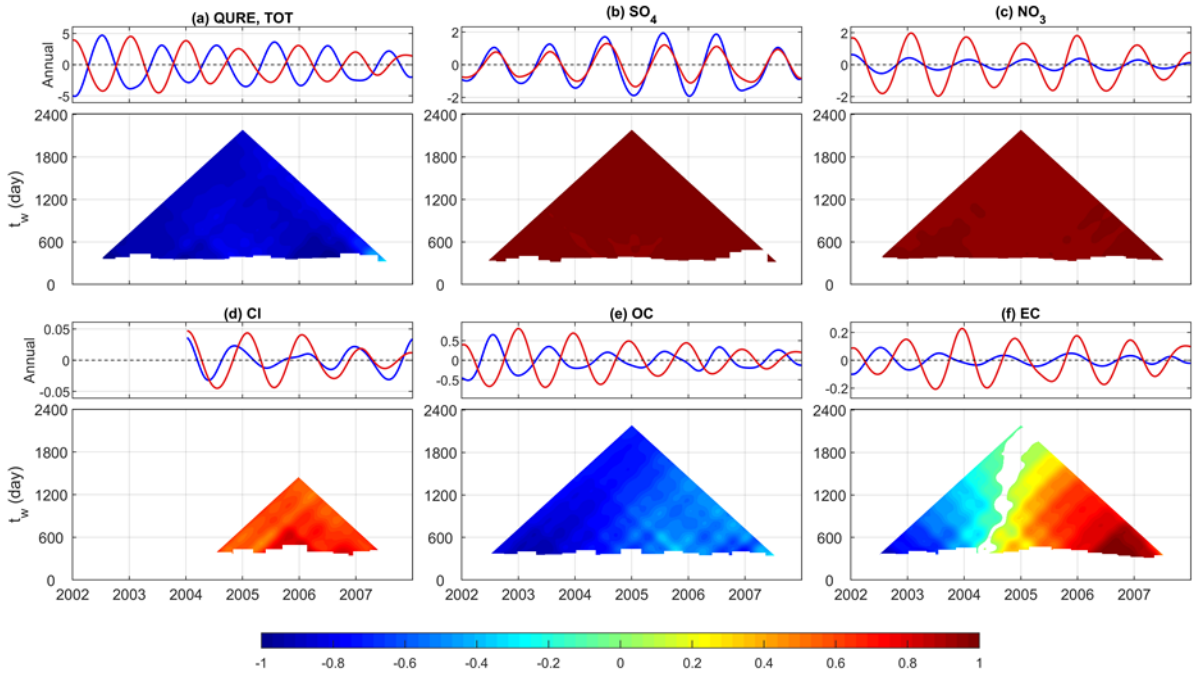

Fig. 7. Decomposed annual cycles (IMF6) from observed (blue) and simulated (red) concentrations (μg/m^3) of (a) total $PM_{2.5}$, (b) SO_4, (c) NO_3, (d) Cl, (e) OC, and (f) EC and their corresponding TDIC at Quabbin Summit, MA. The window size t_w indicates the width of the window used to calculate a specific correlation centered at the day represented in x-axis.

What are the driving factors for the above phase shift in modeled total $PM_{2.5}$ at Quabbin Summit, MA? The illustrations in Fig. 7a for total $PM_{2.5}$ alone cannot provide useful information that will allow the modeler to improve the model's performance. This is accomplished by applying the EMD method to the $PM_{2.5}$ speciated components (Fig. 7b-f). Traces of the semi-annual phase shift (-159 days) of annual cycles or large overestimation in the winter and underestimation in the summer is because of the largely overestimated amplitude of NO_3 (4.3 times that of observation) which peaks in the winter and the almost semi-annual shifted OC (-147 days), as well as contributions from EC and Cl. NO_3 has a mean amplitude reaching almost half of that of the total $PM_{2.5}$. OC directly drives both the observed and simulated annual components to be negatively correlated. EC follows the feature of OC in the first four years or so and the feature of NO_3 in 2006 and 2007 and contributes to the half year shifted total $PM_{2.5}$. The magnitude of winter-peaking Cl cycles is overestimated with a phase shift of one month. However, the contribution of Cl is very limited because of the tiny amplitude in both observed and simulated annual cycles. In addition, annual cycles in SO_4 are well reproduced for the entire time span with an amplitude ratio of 0.7. A quantitative summary of the evaluation of the annual cycles at this site can be found in Tables 3 and 4.

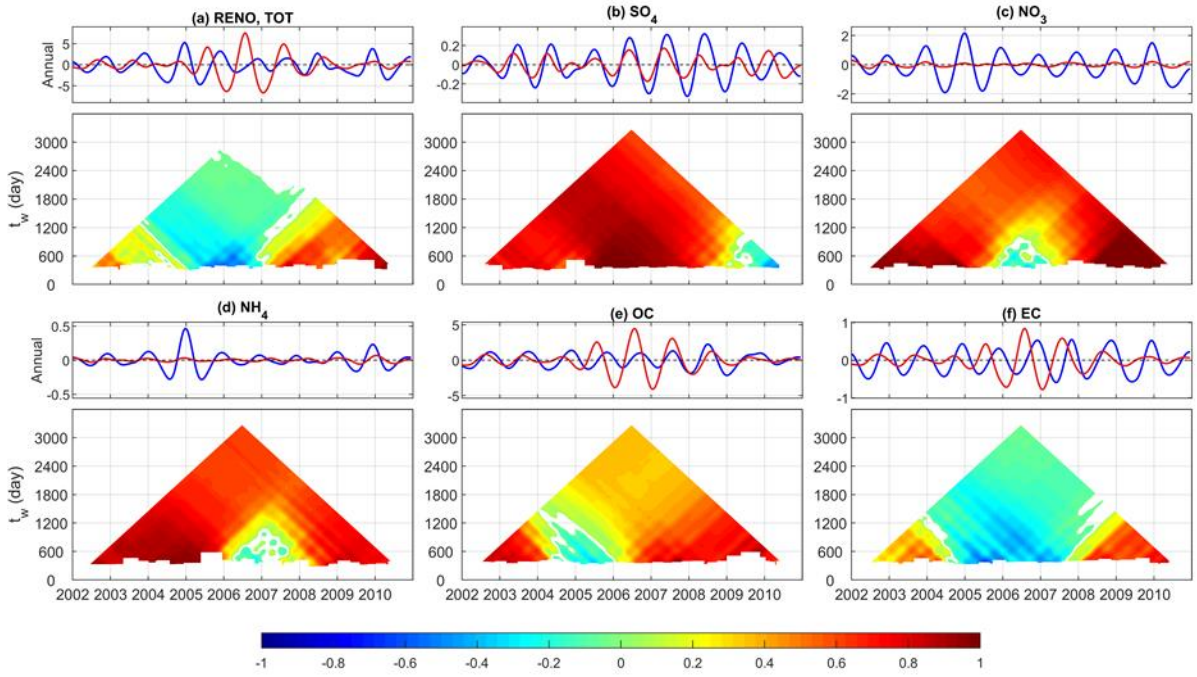

Fig. 8. Same as in Fig. 7 for Reno, NV, except that (d) represents NH_4 rather than Cl.

Both observed and simulated annual cycles at the RENO site are largely influenced by the extreme events lasting for several months that are not properly simulated, indicating the need for more accurately specified wildfire emissions. Overall, annual variations for total and speciated $PM_{2.5}$ are largely underestimated except for the total $PM_{2.5}$ and combustion-driven EC and OC from 2005 to 2007 (Fig. 8). The modeled phase of SO_4, NO_3, NH_4, and OC agrees with that of observation with the exception for a length of about two years in each that missed the phasing: 2009-2010 for SO_4, summer 2005-summer 2007 for NO_3, 2006-2007 for NH_4, and 2004-2005 for OC. It is also notable that the TDIC pyramid of EC mimics that of total $PM_{2.5}$, implying the existence of errors in modeled EC in processes such as emissions, transport, and deposition that affected the model performance for total $PM_{2.5}$. In comparison, SO_4 and OC are relatively well simulated with a mean amplitude ratio of 0.5 and 1.5 and a phase shift of 36 and 33 days, respectively.

Observed annual cycles of total $PM_{2.5}$ at the ATL site features a slightly increasing amplitude of annual variations from 2002 to 2006 which then decreased to the original state in 2007 (Fig. 9a). Conversely, model-simulated annual cycles became weaker throughout the period, with an overall r_{annual} of 0.5. As at the QURE site, the simulated annual components at the ATL site also show a shift of several months (-132 days). Specifically, traces of these phase shifts or large overestimation in the winter and underestimation in the summer can be seen from the more than doubled amplitude of NO_3 which peaks in winter and underestimated SO_4 and NH_4 in the warm seasons as well as the -54 days shifted EC. The anti-correlated remaining species other than those in the available dataset clearly played a role in driving the discrepancies seen in the total $PM_{2.5}$ annual cycles (Fig. 10). Specifically, the anti-correlation likely points to an inaccurate representation of the seasonal variation of the non-carbonaceous portion of organic matter due to an incomplete representation of organic aerosols in the model version analyzed here; newer versions of the CMAQ model

include updated treatment of organic aerosols (e.g., additional SOA formation pathways, improvements in representation of primary OM emissions) which is likely to improve the mentioned features (Appel et al., 2017; Murphy et al., 2017; Xu et al., 2018). The underestimated annual variations in the remaining components closely resemble that of the annual variation in total $PM_{2.5}$. The phase of simulated SO_4, NO_3, NH_4, and OC species is in good agreement with those in observations and the amplitude of simulated annual cycles in SO_4, OC, and EC agree well with that in the observations (Tables 3 and 4).

In sum, annual cycles of $PM_{2.5}$ are also time-dependent and the phase in the annual cycles for total $PM_{2.5}$, OC, and EC reveals a general shift of up to half a year (Table 4); this indicates a potential problem in the allocation of emissions during this study period and/or the treatment of organic aerosols in this version of the model. CMAQ generally simulated the phase in SO_4, NO_3, Cl, and NH_4 quite well but did not always capture the magnitude of their variations (Table 3).

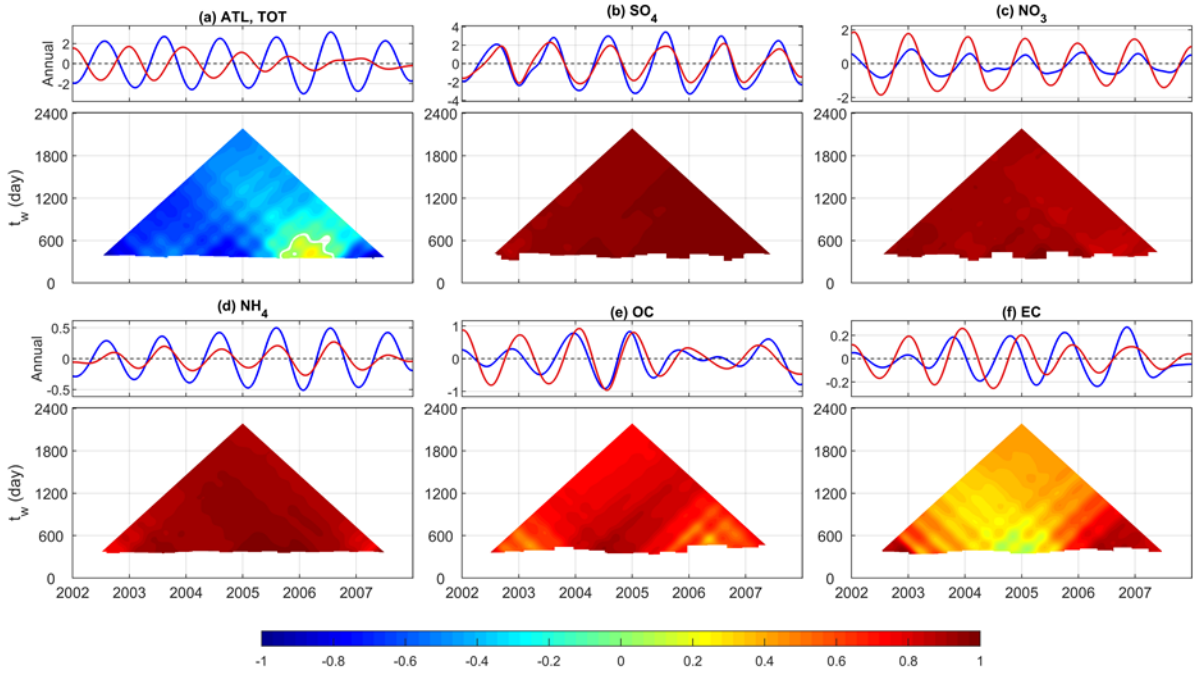

Fig. 9. Same as in Fig. 7 for Atlanta, GA, except that the annual component is resolved in IMF8 (IMF7 for SO_4 and NO_3) because of the difference in sampling rate and characteristic embedded in the time series at ATL and (d) represents NH_4 rather than Cl.

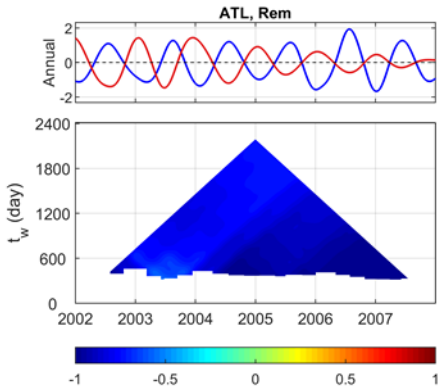

Fig. 10. Decomposed annual cycles in Atlanta, GA for the remaining components presented in total $PM_{2.5}$ other than the five species in Fig.9.

Table 3. The ratio of mean amplitude of the annual component r_{annual} (CMAQ/observation). Boldface values indicate a magnitude with a ratio close to 1 (0.7 -1.3).

	TOT	SO_4	NO_3	NH_4	OC	EC	Cl
QURE	**1.0**	**0.7**	4.3	-	1.6	3.1	1.6
RENO	**1.2**	0.5	0.1	0.2	1.5	**0.9**	-
ATL	0.5	**0.7**	2.4	0.4	**1.2**	**1.0**	-

Table 4. Phase shift (n) of CMAQ simulated annual cycle components in days. The background color indicates the maximum correlation (R_{max}) that can be reached by shifting the CMAQ time series n days with respect to observations: white = [0.8, 1], light grey = [0.6, 0.8), grey = [0.4, 0.6), dark grey = (0.2, 0.4). The bold shows number of shifts less than a month while the italic shows shifts longer than three months.

	TOT	SO_4	NO_3	NH_4	OC	EC	Cl
QURE	*-159*	**-6**	**3**	**-**	*-147*	*-105*	**-30**
RENO	78	36	**12**	**-21**	33	*96*	-
ATL	*-132*	**0**	**8**	**-17**	**-24**	-54	-

4.4 Sub-seasonal and inter-annual variability

In this section, model performance at multiple sub-seasonal and inter-annual scales with cycles less than 3 years, presented in the total and speciated $PM_{2.5}$, is evaluated following an approach similar to that for the annual cycles in Section 4.3 (Fig. 11). First, IMFs from observations and model simulations are paired based on their characteristic periods following the discussion in Section 4.1. Then, the magnitude of specific scales is evaluated using r_{IMFn} following Equation 6 of the r_{annual} for annual cycles. The phase shifts of the time series are assessed by the proportion of shifted days relative to the mean characteristic scales of the corresponding observed and simulated IMFs ($^{n}/_{t_m}$).

For example, a phase shift of 0.1 cycles in the 2-year cycles is approximately 73 days while it would be 18 days for the half-year cycles.

The performance of the simulated amplitude of the sub-seasonal and inter-annual cycles is relatively stable from a few days to semi-annual scales and r_{IMFn} is close to 1 in most cases (Fig. 11a-c). CMAQ captures the features seen in the observations at QURE, except for the large overestimation of NO_3 (r_{IMFn} ranges from 2.6 to 3.7 at the sub-seasonal scale and reaches up to 13.8 for the 3-year cycles). Similar overestimation of NO_3 is also found at ATL (r_{IMFn} ranges from 2.0 to 3.4, except for the 2-year cycles). In contrast, NO_3 at RENO is strongly underestimated with r_{IMFn} ranging from 0.1 to 0.3 and reaching its minimum at the 2-year cycles. Likewise, all time scales of NH_4 at RENO are also being underestimated with r_{IMFn} decreasing from 0.4 to only 0.1 at the 3-year cycles. The coexistence of underestimation of NO_3 and NH_4 variability, as well as their trend component, likely points to the insufficient grid resolution in representing ammonium nitrate episodes associated with stagnant meteorology in the mountainous regions as illustrated by Kelly et al. (2019). To sum up, model has simulated the magnitude of features across all scales in most of the studied cases. However, fluctuations in NO_3 are constantly being largely over- or under-estimated and improvements to the model are required to better replicate its variability (Fig. 11a-c).

A high R_{max} of corresponding IMFs can only be achieved when the characteristic scales of those from observations and model simulations are close, there is minimal mode mixing, and negligible irregular change of amplitude exists during the study period. Thus, R_{max} tends to be small for all oscillations at RENO because of the irregular impact from events such as wildfires. Thus, the interpretation of phase shift is focused on the components and time scales having correlations above 0.4 only.

Results show that the sub-seasonal cycles at QURE all have a negligible phase shift of less than 0.1 cycles (Fig. 11d). The semi-annual cycles at RENO have around 0.2 cycle phase shifts in total $PM_{2.5}$ (-0.2), NH_4(0.2), OC (-0.2), and EC (-0.2) while negligible phase shifts of less than 0.1 cycles are simulated in SO_4 ranging from 9 days to semi-annual in scale. As at QURE, multiple sub-seasonal cycles at ATL all have a negligible phase shift of less than 0.1 cycles, with the exception of semi-annual OC which has a phase shift of nearly -0.4 cycles with a marginal correlation of around 0.4. Unlike the relatively stable R_{max} throughout the time scales within each of the species for QURE and RENO, the R_{max} at ATL tends to be much higher (roughly 0.6-0.8) in the scales of 6 to 25 days, except for NO_3, indicating the model's success in simulating those weather-induced air quality fluctuations at this site as reflected by their negligible phase shifts.

However, the physical meaning of each sub-seasonal IMF is not yet fully understood and requires further study. For example, synoptic scale IMFs (IMFs with scale less than/around a month) usually have large variance and are not statistically significantly different from white noise except for observed SO_4 and NH_4 (Fig. S5). Yet, observed and simulated total and some speciated $PM_{2.5}$ at QURE and ATL (except IMF1) can achieve moderate to high R_{max} at these time scales (Fig. 11 g-i), indicating a potential physical explanation of those time scales using meteorological variables. IMFs with scales longer than a month but less than half year possess much less variance and are usually not statistically significantly different from noise. Exceptions are also found at the Atlanta site where observed IMFs are

mostly significantly different from noise. Whereas semi-annual cycles are mostly statistically significant (note that semi-annual SO_4 and NO_3 at ATL are too weak to be decomposed into a separate IMF). In a previous study, He et al. (2014) found semi-annual oscillations in the corrected AErosol RObotic NETwork (AERONET) Aerosol Optical Depth (AOD) and PM_{10} mass concentrations are primarily caused by the change of wind directions in Hong Kong.

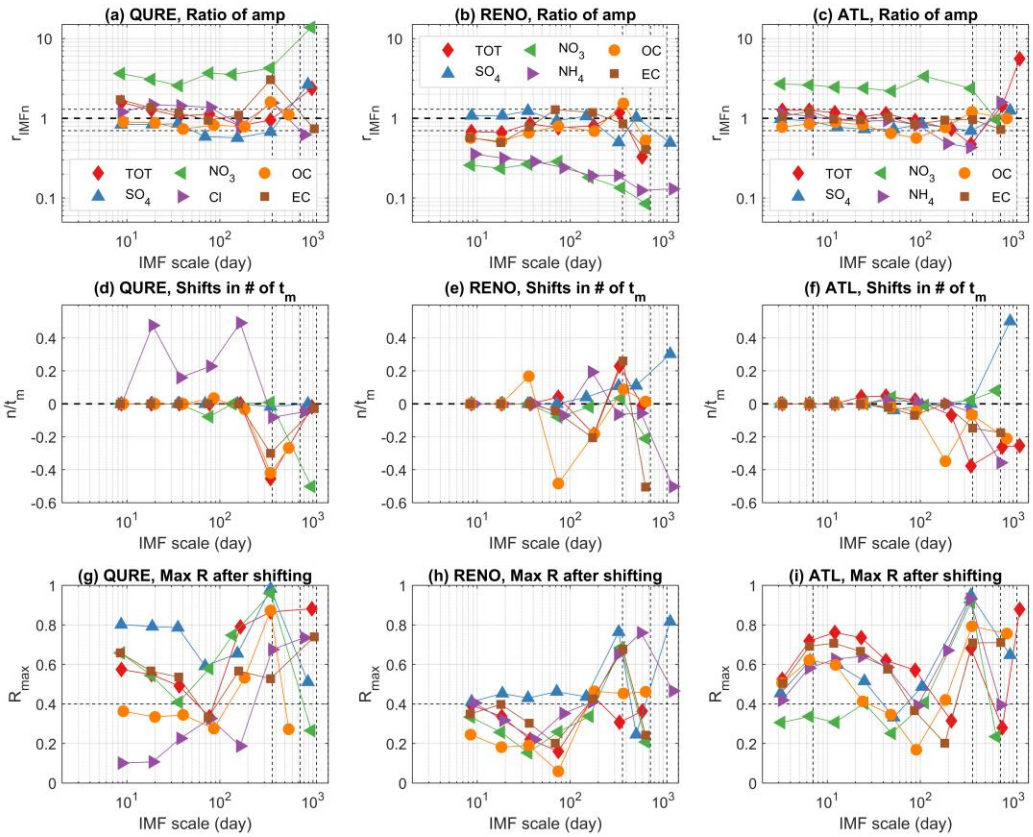

Fig. 11. Model performance at all temporal scales for sites QURE, RENO, and ATL. (a-c) ratio of mean amplitude of corresponding IMFs with similar characteristic mean periods (ideal ratio=1.0); (d-f) the phase shift n in the number of mean periods (average mean period of corresponding IMFs decomposed from observation and model simulation); (g-i) maximum correlation R_{max} can be achieved by shifting the modeled time series. The average mean period of corresponding IMFs decomposed from observations and CMAQ of total and speciated $PM_{2.5}$ are represented on the x-axis; all metrics on the y-axis are unitless. Horizontal reference lines are drawn at 0.7 and 1.3 in (a-c). Weekly, annual, and inter-annual (2- to 3-year) scales are marked with vertical dashed lines.

The evaluation and interpretation of inter-annual cycles are constrained by the limited available speciated observations for a period of 6 to 9 years (4 years for Cl at QURE). Thus, only 2- to 3-year cycles are presented (Fig. 11) and evaluated. Among the 2- to 3-year inter-annual cycles at QURE, there is minimal phase shift for total $PM_{2.5}$, SO_4, Cl, and EC with moderate to high R_{max}. At RENO, the model presents negligible shifts in 2-year cycles of OC and NH_4

while phase shifts of 0.3 and -0.5 cycles are simulated in the 3-year cycles for SO_4 and NH_4. At ATL, the phase shift of -0.2 to -0.4 cycles are simulated for $PM_{2.5}$, NH_4, OC, and EC with periods of 2- to 3-year cycles; while 2- to 3-year SO_4 cycles have a half-year cycle shift.

5 Conclusions

The main advantage for using EMD to evaluate $PM_{2.5}$ and its speciated components is that it decomposes nonlinear and nonstationary signals into multiple modes and a residual trend component. It does not require any preselection of the temporal scales and assumptions of linearity and stationarity for the data, thereby providing insights into time series of $PM_{2.5}$ concentrations and its components. Using improved CEEMDAN, we are able to assess how well regional-scale air quality models like CMAQ can simulate the intrinsic time-dependent long-term trend and cyclic variations in daily average $PM_{2.5}$ and its species. This type of coordinated decomposition and evaluation of total and speciated $PM_{2.5}$ provides a unique opportunity for modelers to assess influences of each $PM_{2.5}$ species to the total $PM_{2.5}$ concentration in terms of time shifts for various temporal cycles and the magnitude of each component including the trend.

A demonstration of how improved CEEMDAN could be applied to $PM_{2.5}$ time series at three sites over CONUS that provide speciated $PM_{2.5}$ data reveals the presence of the annual cycles in $PM_{2.5}$ concentrations and time-dependent features in all decomposed components. At these three sites, the model generally is more capable of simulating the change rate in the trend component than the absolute magnitude of the long-term trend component. However, the magnitude of SO_4 trend components is well represented across all three sites. Also, the model reproduced the amplitude of the annual cycles for total $PM_{2.5}$, SO_4, and OC. The phase difference in the annual cycles for total $PM_{2.5}$, OC, and EC reveal a shift of up to half year, indicating the need for proper allocation of emissions and an updated treatment of organic aerosols compared to the earlier model version used in this set of model simulations. The consistent large under/over-prediction of NO_3 variability at all temporal scales and magnitude in the trend component, as well as the abnormally low correlations of synoptic scale NO_3 at ATL, calls for better representation of nitrate partitioning and chemistry. Wildfires have the potential to elevate $PM_{2.5}$ for months and can alter its variability at scales from few days to the entire year. Thus, more accurate fire emission data should be incorporated to improve model simulation, especially in those fire-prone regions.

Data availability. Paired observations and CMAQ model data used in the analysis will be made available at https://edg.epa.gov/metadata/catalog/main/home.page. Raw CMAQ model outputs are available on request from the U.S. EPA authors.

Author contribution. "HL and MA designed the methodology; RM, CH, and SR contributed in the assessment of the outcomes and were consulted on necessary revisions. Model simulations were performed by the US EPA. HL prepared the manuscript with contributions from all co-authors."

Acknowledgements

The views expressed in this paper are those of the authors and do not necessarily represent the view or policies of the U.S. Environmental Protection Agency. Two of the authors (MA and HL) acknowledge that part of this work was supported by the Electric Power Research Institute (EPRI) Contract #00-10005071, 2015–2017.

References

Appel, K.W., Napelenok, S.L., Foley, K.M., Pye, H.O., Hogrefe, C., Luecken, D.J., Bash, J.O., Roselle, S.J., Pleim, J.E., Foroutan, H. and Hutzell, W.T., 2017. Description and evaluation of the Community Multiscale Air Quality (CMAQ) modeling system version 5.1. Geoscientific Model Development, 10(4), p.1703.

Astitha, M., Luo, H., Rao, S.T., Hogrefe, C., Mathur, R., Kumar, N., 2017. Dynamic evaluation of two decades of WRF-CMAQ ozone simulations over the contiguous United States. Atmospheric Environment 164, 102–116.

Banzhaf, S., Schaap, M., Kraneburg, R., Manders, A.M.M., Segers, A.J., Visschedijk, A.H.J., Denier van der on, H.A.C., Kuenen, J.P.P., van Meijgaard, E., van Ulft, L.H., Cofala, J., Builtjes, P.J.H., 2015. Dynamic model evaluation for secondary inorganic aerosol and its precursors over Europe between 1990 and 2009. Geoscientific Model Development 8, 1047–1070.

Chang, P.C., Flatau, A., Liu, S.C., 2003. Review Paper: Health Monitoring of Civil Infrastructure. Structural Health Monitoring 2, 257–267.

Chen, X., Wu, Z., Huang, N.E., 2010. The time-dependent intrinsic correlation based on the empirical mode decomposition. Adv. Adapt. Data Anal. 02, 233–265.

Civerolo, K., Hogrefe, C., Zalewsky, E., Hao, W., Sistla, G., Lynn, B., Rosenzweig, C., Kinney, P.L., 2010. Evaluation of an 18-year CMAQ simulation: Seasonal variations and long-term temporal changes in sulfate and nitrate. Atmospheric Environment 44, 3745–3752.

Colominas, M.A., Schlotthauer, G., Torres, M.E., 2014. Improved complete ensemble EMD: A suitable tool for biomedical signal processing. Biomedical Signal Processing and Control 14, 19–29.

Derot, J., Schmitt, F.G., Gentilhomme, V., Morin, P., 2016. Correlation between long-term marine temperature time series from the eastern and western English Channel: Scaling analysis using empirical mode decomposition. Comptes Rendus Geoscience 348, 343–349.

Edgerton, E.S., Hartsell, B.E., Saylor, R.D., Jansen, J.J., Hansen, D.A., Hidy, G.M., 2005. The Southeastern Aerosol Research and Characterization Study: Part II. Filter-Based Measurements of Fine and Coarse Particulate Matter Mass and Composition. Journal of the Air & Waste Management Association 55, 1527–1542.

Foley, K.M., Hogrefe, C., Pouliot, G., Possiel, N., Roselle, S.J., Simon, H., Timin, B., 2015. Dynamic evaluation of CMAQ part I: Separating the effects of changing emissions and changing meteorology on ozone levels between 2002 and 2005 in the eastern US. Atmospheric Environment 103, 247–255.

Gan, C.-M., Pleim, J., Mathur, R., Hogrefe, C., Long, C.N., Xing, J., Wong, D., Gilliam, R., Wei, C., 2015. Assessment of long-term WRF–CMAQ simulations for understanding direct aerosol effects on radiation "brightening" in the United States. Atmospheric Chemistry and Physics 15, 12193–12209.

Gyawali, M., Arnott, W.P., Lewis, K. and Moosmüller, H., 2009. In situ aerosol optics in Reno, NV, USA during and after the summer 2008 California wildfires and the influence of absorbing and non-absorbing organic coatings on spectral light absorption. Atmospheric Chemistry & Physics, 9(20).

Hansen, D.A., Edgerton, E.S., Hartsell, B.E., Jansen, J.J., Kandasamy, N., Hidy, G.M., Blanchard, C.L., 2003. The Southeastern Aerosol Research and Characterization Study: Part 1—Overview. Journal of the Air & Waste Management Association 53, 1460–1471.

He, J., Zhang, M., Chen, X., & Wang, M., 2014. Inter-comparison of seasonal variability and nonlinear trend between AERONET aerosol optical depth and PM10 mass concentrations in Hong Kong. Science China Earth Sciences, 57(11), 2606-2615.

Henneman, L.R.F., Liu, C., Hu, Y., Mulholland, J.A., Russell, A.G., 2017. Air quality modeling for accountability research: Operational, dynamic, and diagnostic evaluation. Atmospheric Environment 166, 551–565.

Hogrefe, C., Hao, W., Zalewsky, E.E., Ku, J.-Y., Lynn, B., Rosenzweig, C., Schultz, M.G., Rast, S., Newchurch, M.J., Wang, L., Kinney, P.L., Sistla, G., 2011. An analysis of long-term regional-scale ozone simulations over the Northeastern United States: variability and trends. Atmospheric Chemistry and Physics 11, 567–582.

Huang, N.E., Shen Zheng, Long Steven R., Wu Manli C., Shih Hsing H., Zheng Quanan, Yen Nai-Chyuan, Tung Chi Chao, Liu Henry H., 1998. The empirical mode decomposition and the Hilbert spectrum for nonlinear and non-stationary time series analysis. Proceedings of the Royal Society of London. Series A: Mathematical, Physical and Engineering Sciences 454, 903–995.

Huang, Y., Schmitt, F.G., 2014. Time dependent intrinsic correlation analysis of temperature and dissolved oxygen time series using empirical mode decomposition. Journal of Marine Systems 130, 90–100.

Kang, D., Hogrefe, C., Foley, K.L., Napelenok, S.L., Mathur, R., Trivikrama Rao, S., 2013. Application of the Kolmogorov–Zurbenko filter and the decoupled direct 3D method for the dynamic evaluation of a regional air quality model. Atmospheric Environment 80, 58–69.

Kelly, J.T., Koplitz, S.N., Baker, K.R., Holder, A.L., Pye, H.O.T., Murphy, B.N., Bash, J.O., Henderson, B.H., Possiel, N.C., Simon, H., Eyth, A.M., Jang, C., Phillips, S., Timin, B., 2019. Assessing PM2.5 model performance for the conterminous U.S. with comparison to model performance statistics from 2007-2015. Atmospheric Environment 214, 116872.

Mathur, R., Xing, J., Gilliam, R., Sarwar, G., Hogrefe, C., Pleim, J., Pouliot, G., Roselle, S., Spero, T.L., Wong, D.C., Young, J., 2017. Extending the Community Multiscale Air Quality (CMAQ) Modeling System to Hemispheric Scales: Overview of Process Considerations and Initial Applications. Atmos Chem Phys 17, 12449–12474.

606 Moghtaderi, A., Borgnat, P., Flandrin, P., 2012. Gap-filling by the empirical mode decomposition, in: 2012 IEEE
607 International Conference on Acoustics, Speech and Signal Processing (ICASSP). Presented at the 2012 IEEE
608 International Conference on Acoustics, Speech and Signal Processing (ICASSP), pp. 3821–3824.

609 Murphy, B.N., Woody, M.C., Jimenez, J.L., Carlton, A.M.G., Hayes, P.L., Liu, S., Ng, N.L., Russell, L.M., Setyan,
610 A., Xu, L. and Young, J., 2017. Semivolatile POA and parameterized total combustion SOA in CMAQv5. 2: impacts
611 on source strength and partitioning. Atmospheric Chemistry and Physics, 17, p.11107.

612 Rato, R.T., Ortigueira, M.D., Batista, A.G., 2008. On the HHT, its problems, and some solutions. Mechanical Systems
613 and Signal Processing, Special Issue: Mechatronics 22, 1374–1394.

614 Torres, M.E., Colominas, M.A., Schlotthauer, G., Flandrin, P., 2011. A complete ensemble empirical mode
615 decomposition with adaptive noise, in: 2011 IEEE International Conference on Acoustics, Speech and Signal
616 Processing (ICASSP). Presented at the 2011 IEEE International Conference on Acoustics, Speech and Signal
617 Processing (ICASSP), pp. 4144–4147.

618 White, W.H., 2008. Chemical markers for sea salt in IMPROVE aerosol data. Atmospheric Environment 42, 261–
619 274.

620 Wong, D.C., Pleim, J., Mathur, R., Binkowski, F., Otte, T., Gilliam, R., Pouliot, G., Xiu, A., Young, J.O., Kang, D.,
621 2012. WRF-CMAQ two-way coupled system with aerosol feedback: software development and preliminary results.
622 Geoscientific Model Development 5, 299–312.

623 Wu, Z., Huang, N.E., 2004. A study of the characteristics of white noise using the empirical mode decomposition
624 method. Proceedings of the Royal Society of London. Series A: Mathematical, Physical and Engineering Sciences
625 460, 1597–1611.

626 Wu, Z., Huang, N.E., 2009. Ensemble empirical mode decomposition: a noise-assisted data analysis method. Adv.
627 Adapt. Data Anal. 01, 1–41.

628 Wu, Z., Huang, N.E., Long, S.R., Peng, C.-K., 2007. On the trend, detrending, and variability of nonlinear and
629 nonstationary time series. PNAS 104, 14889–14894.

630 Xing, J., Mathur, R., Pleim, J., Hogrefe, C., Gan, C.-M., Wong, D.C., Wei, C., Gilliam, R., Pouliot, G., 2015.
631 Observations and modeling of air quality trends over 1990–2010 across the Northern Hemisphere: China, the United
632 States and Europe. Atmospheric Chemistry and Physics 15, 2723–2747.

633 Xing, J., Pleim, J., Mathur, R., Pouliot, G., Hogrefe, C., Gan, C.-M., Wei, C., 2013. Historical gaseous and primary
634 aerosol emissions in the United States from 1990 to 2010. Atmospheric Chemistry and Physics 13, 7531–7549.

635 Xu, L., Pye, H.O., He, J., Chen, Y., Murphy, B.N. and Ng, L.N., 2018. Experimental and model estimates of the
636 contributions from biogenic monoterpenes and sesquiterpenes to secondary organic aerosol in the southeastern United
637 States. Atmospheric chemistry and physics, 18(17), p.12613.

638 Yahya, K., Wang, K., Campbell, P., Glotfelty, T., He, J., Zhang, Y., 2016. Decadal evaluation of regional climate, air
639 quality, and their interactions over the continental US using WRF/Chem version 3.6.1. Geoscientific Model
640 Development 9, 671–695.

641 Yeh, J.-R., Shieh, J.-S., Huang, N.E., 2010. Complementary ensemble empirical mode decomposition: a novel noise
642 enhanced data analysis method. Adv. Adapt. Data Anal. 02, 135–156.

643 Yu, L., Wang, S., Lai, K.K., 2008. Forecasting crude oil price with an EMD-based neural network ensemble learning
644 paradigm. Energy Economics 30, 2623–2635.

645 Zhou, W., Cohan, D.S., Napelenok, S.L., 2013. Reconciling NOx emissions reductions and ozone trends in the U.S.,
646 2002–2006. Atmospheric Environment 70, 236–244.

647